THE JOURNAL OF PHYSICAL CHEMISTRY C
A JOURNAL OF THE AMERICAN CHEMICAL SOCIETY

pubs.acs.org/JPCC
Article

Engineering the Effective Mass in 2D Perovskites via Octahedral Distortion

Paulina Peksa, Arthur Maufort, Michał Baranowski, Alessandro Surrente, Laurence Lutsen, Paulina Płochocka, Wouter T. M. Van Gompel, and Mateusz Dyksik*

Cite This: J. Phys. Chem. C 2024, 128, 17984−17989
Read Online

ACCESS | Metrics & More | Article Recommendations | Supporting Information

ABSTRACT: Two-dimensional (2D) perovskites are well-known for the broad tunability of their optoelectronic properties. One of the prime methods is templating the inorganic sublattice via a selection of organic spacers. Here, with the use of magneto-optical spectroscopy, we demonstrate the remarkable potential of distortion engineering to tune the effective mass in 2D perovskites. We show that the 2D perovskites containing benzotriazole-based organic cations are characterized by the lowest reduced effective mass that has been measured for a lead iodide 2D perovskite. This stems directly from the very low degree of octahedral distortion in this material system. The practically flat structure of inorganic sublattice with no measurable out-of-plane corrugation results in the reduction of reduced effective mass by 12% with respect to the reference structure of $(PEA)_2PbI_4$. The reduction in the mass is naturally accompanied by a lower 1s exciton binding energy of ∼200 meV.

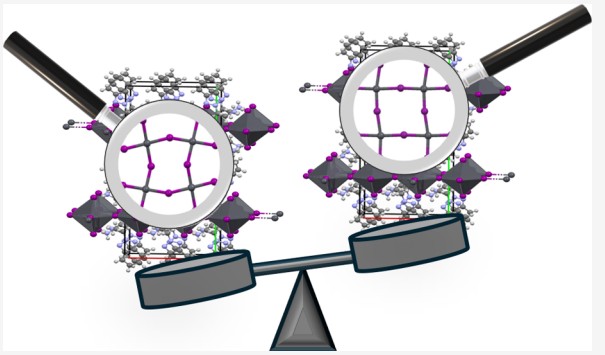

INTRODUCTION

Two-dimensional (2D) layered metal-halide perovskites have raised significant attention as a more stable alternative[1−3] to their three-dimensional (3D) counterparts.[4,5] These natural quantum wells, which consist of octahedral metal-halide slabs separated by large organic spacers, are considered promising candidates for low-cost light emitters and for energy harvesting applications.[5−9] The improved stability of 2D perovskites is related to the hydrophobic nature of the large organic spacers,[5] which also offers an efficient means to tune the optoelectronic properties of these materials.[1,8,10]

An appropriate selection of the organic spacer enables to control the emission and absorption energy,[11,12] the exciton−phonon coupling[13,14] or to tune the effective mass of charge carriers[12,15−17] via octahedral templating (steric effects)[18,19] and dielectric confinement.[20] The latter is of paramount importance because it governs essential physical parameters such as the carrier mobility, the exciton binding energy, and the carrier diffusion length. All of them are crucial for applications as light emitters and in solar cells. In the case of photovoltaic applications, it is expected that a lower carrier mass is beneficial, enhancing diffusion length and reducing exciton binding energy. Therefore, it is very tempting to make use of the templating effect to tune the reduced effective mass, and very interesting to understand to what extent this tuning knob can be used.

Recent theoretical and experimental investigations have shown that both the bandgap and effective mass can be controlled by the octahedral unit distortion angles imposed by the organic spacers.[11,12,15,17,21−24] A simplified scheme of the δ and β distortion angles of the inorganic sublattice is shown in Figure 1a. A precise definition of the δ angle is presented in Figure S1. The lower the distortion angles the lower the effective mass and the band gap.[15] To date, the reduced effective mass μ has been determined for $(PEA)_2PbI_4$ ($\mu \sim 0.091\ m_0$)[15] and $(BA)_2PbI_4$ ($\mu \sim 0.22\ m_0$),[25] where PEA stands for phenylethylammonium and BA stands for butylammonium. The lowest effective mass in the family of PbI_4-based 2D layered perovskites has been reported for $(PEA)_2PbI_4$,[15,16] which primarily stems from a much smaller δ angle when compared with other measured compounds.

Here, we show that the distortion engineering can be pushed even further with the use of benzotriazole-based ammonium cation BTa and its difluorinated derivative F_2BTa. The two corresponding 2D perovskites compounds, $(BTa)_2PbI_4$ (Figure 1b) and $(F_2BTa)_2PbI_4$ (Figure S2a), are synthesized and the cations' structure is presented in Figure 1c. Both samples are characterized by an exceptionally low degree of octahedral distortion[26,27] − the presence of intramolecular hydrogen

Received: August 6, 2024
Revised: October 4, 2024
Accepted: October 4, 2024
Published: October 15, 2024

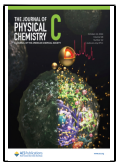

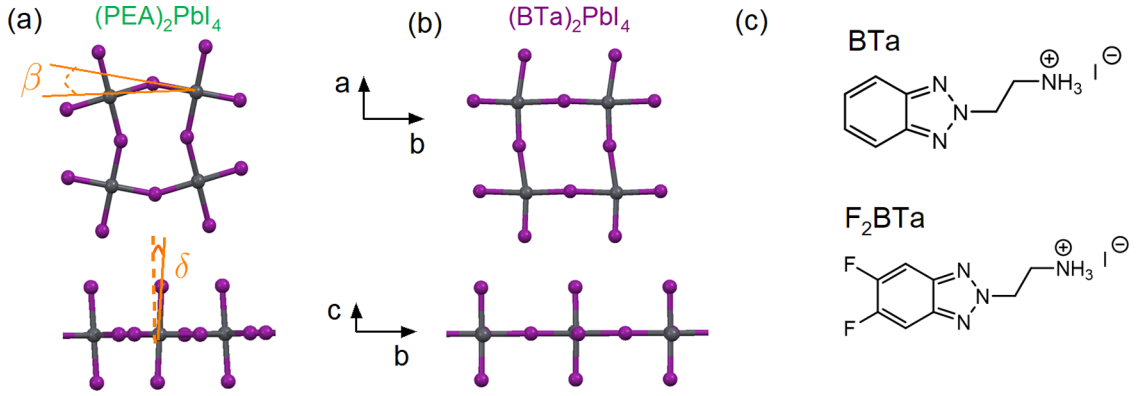

Figure 1. (a) Definition of octahedral distortion angles β and δ. (b) Crystal structure of $(BTa)_2PbI_4$. (c) Benzotriazole organic spacers: BTa (top) and F_2BTa (bottom).[26]

Table 1. Summary of Octahedral Distortion Angles β and δ for Different 2D Layered Perovskite together with Exciton Reduced Mass (μ), Diamagnetic Coefficient (c_0), and Exciton Binding Energy (E_b)[a]

compound	β angle (°)	δ angle (°)	μ (m_0)	c_0 (μeV T^{-2})	E_b (meV)
$(BA)_2PbI_4$	15.38 (LT)12.5 (HT)[28]	12.92 (LT) 5.78 (HT)[28]	0.22[25]	0.13[17]	250−470[25,29]
$(PEA)_2PbI_4$	14[30]	2[31]	0.091[15]	0.36[15]	223−260[15,29]
$(BTa)_2PbI_4$	3.25[26]	0[26]	0.081 ± 0.002	0.41 ± 0.03	206 ± 2
$(F_2BTa)_2PbI_4$	3[26]	0[26]	0.080 ± 0.002	0.44 ± 0.02	208 ± 4

[a]LT: low temperature phase; HT: high temperature phase.

bonding between the ammonium head of the alkylammonium tail and a nitrogen atom of the benzotriazole core results in a negative penetration depth of the ammonium head into the inorganic framework, with minimal distortion of the inorganic framework as a result.[27] In these benzotriazole-based 2D perovskites, the octahedral slab is practically flat (out-of-plane distortion angle δ = 0, see Figure 1b), and the in-plane deviation of the I−Pb−I angle from 180° is much smaller than in the case of $(PEA)_2PbI_4$ or $(BA)_2PbI_4$, which translates to β ∼ 3°. Therefore, a low reduced effective mass and a low exciton binding energy is expected. Our magneto-optical spectroscopy studies up to 86 T confirms this expectation. Both the diamagnetic shift of the excitonic transition and the interband Landau level transitions provide evidence for the lowest reported effective mass in lead-based 2D perovskites (for summary see Table 1). Our studies show that the control of the reduced effective mass in 2D perovskite by the templating effect can be treated as a general strategy, which might also be extended for tin-based 2D perovskite compounds.

MATERIALS AND METHODS

Optical Spectroscopy Setup. Reflectivity spectra as a function of the magnetic field were measured in a pulsed field magnet with a maximum field of 86 T and pulse duration of ∼100 ms. A UV lamp was used to provide broad-band white light. The light was directed to the sample using an optical fiber. The reflected signal was collected by a fiber bundle and guided back to the detection system. The signal was spectrally dispersed using the grating of a monochromator and detected using a liquid-nitrogen-cooled CCD camera. The sample was placed in a liquid helium cryostat situated inside the magnet. The photoluminescence excitation (PLE) experimental results have been obtained at cryogenic temperatures of ∼4 K, by cooling down the sample mounted on the coldfinger of a He flow cryostat. A pulsed Ti-sapphire laser was used to pump an optical parametric oscillator, which was used as the tunable excitation source. The laser was focused on the sample with a 50× objective having a numerical aperture of 0.55. The photoluminescence signal was collected by the same objective and directed toward a spectrograph equipped with a liquid nitrogen cooled CCD detector.

Sample Synthesis Details. Single crystals of all perovskites were synthesized as reported in ref 27. Stoichiometric amounts of the organic lead halide were dissolved in a mixture of propylene carbonate (PC), water, and HI (57% in water). HI was extracted three times with a 9:1 (v/v) mixture of chloroform and tri-n-butyl phosphate before use. Lead iodide-based mixtures were stirred at 50 °C until a clear solution was obtained. The solutions were then filtered through a syringe filter into a base-bath cleaned glass vial and were heated to their crystallization temperature. The lid of the vial was perforated with a needle to enable CO_2 to escape during the solvent degradation process. $(BTa)_2PbI_4$ and $(F_2BTa)_2PbI_4$ crystallized as orange needles.[27]

RESULTS AND DISCUSSION

Figure 2a shows the comparison of the reflectivity spectra of a reference $(PEA)_2PbI_4$ and $(BTa)_2PbI_4$ samples, both measured at T = 4 K. For both samples we observe the typical line shape for 2D layered perovskites.[14,30,32−34] For $(PEA)_2PbI_4$ the signal (green line) related to the 1s excitonic transition is visible at 2.36 eV, marked by an arrow, followed by the broad high-energy sideband spanning up to ∼2.42 eV related to the phonon replica/polaronic effects.[14,33,35−37] By analogy, for $(BTa)_2PbI_4$ we assign the 1s exciton transition energy at 2.31 eV (the corresponding reflectivity spectrum of $(F_2BTa)_2PbI_4$ is shown in Figure S2b in Supporting Information). The change of organic spacer results in the red shift of the excitonic transition by approximately 50 meV, due to lower distortions imposed on the octahedral units.[11,26,38] This general trend is summarized in Figure 2b, where the 1s exciton energy is

https://doi.org/10.1021/acs.jpcc.4c05300
J. Phys. Chem. C 2024, 128, 17984−17989

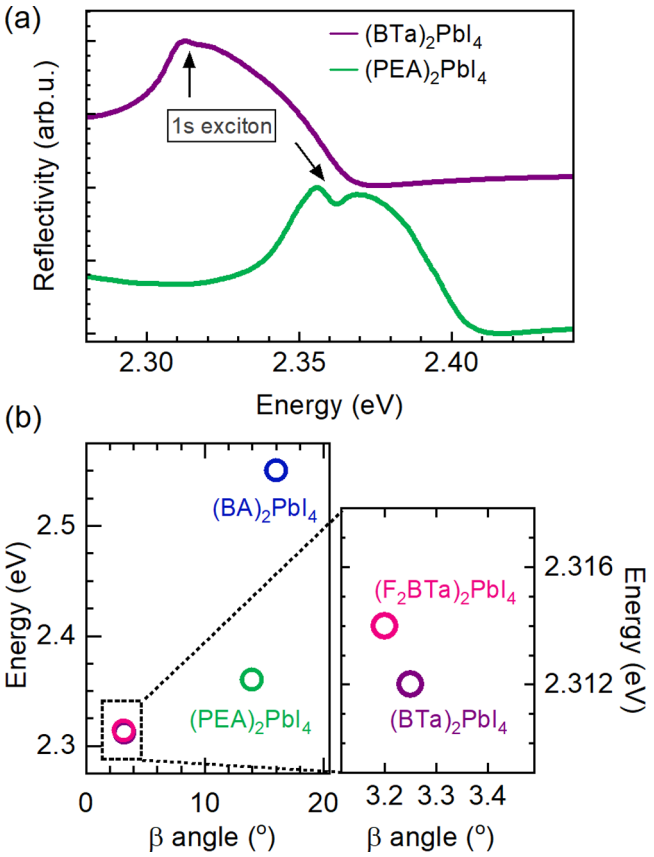

Figure 2. (a) Reflectivity spectrum of $(BTa)_2PbI_4$ and $(PEA)_2PbI_4$. Arrows indicate 1s excitonic transitions. (b) 1s exciton transition energy versus distortion angle β for $(BA)_2PbI_4$ (low temperature phase),[28] $(PEA)_2PbI_4$,[30] $(BTa)_2PbI_4$[26] and $(F_2BTa)_2PbI_4$.[26]

plotted as a function of the distortion angle β for several perovskite compounds.

Typically for semiconductors the reduction of the optical bandgap correlates with the reduction of the effective mass.[39] To directly measure this quantity via Landau level spectroscopy, we performed reflectivity measurements in magnetic fields up to 86 T (for experimental details, see section Materials and Methods). Figure 3a shows the evolution of the reflectivity ratio spectrum (spectrum at a given magnetic field B divided by spectrum measured at 0 T) of $(BTa)_2PbI_4$ at different magnetic fields (similar data for $(F_2BTa)_2PbI_4$ are summarized in Figure S3 in SI).

In the reflectivity ratio spectra, we observe the characteristic resonance-like optical transitions emerging at high magnetic fields above 2.6 eV as detailed in Figure S4. These features, labeled $N = 0$, $N = 1$, and $N = 2$ in Figure 3a, are not visible without the magnetic field, but gain intensity and blue-shift with increasing magnetic field. This behavior is characteristic of the optical transitions between Landau levels with the same orbital quantum number N formed in the valence and conduction band.[15,16,39]

By a careful analysis of the reflectivity ratio spectra $R(B)/R(0T)$ and their derivative (see Figure S5 in SI), we follow the energy evolution of interband Landau level transitions. The resulting optical transition energies are presented in Figure 3b as a function of the magnetic field, yielding a fan chart graph.

Assuming a parabolic band dispersion, the magnetic field dependence of the interband Landau levels transition $E_N(B)$ reads

$$E_N(B) = E_g + \left(N + \frac{1}{2}\right)\hbar\omega_c \tag{1}$$

where E_g is the band gap, N is the Landau orbital quantum number in the conduction and valence band, $\hbar\omega_c = \frac{eB}{\mu}$ is the cyclotron energy, and μ is the exciton reduced mass, $1/\mu = 1/\mu_e + 1/\mu_h$.[15,39] To determine the reduced effective mass μ, we analyze the energy difference ΔE between consecutive Landau levels E_{N+1} and E_N. With this approach, we eliminate the uncertainty of band gap energy. Based eq 1, we obtain

$$\Delta E(B) = \hbar\omega_c = \hbar\frac{eB}{\mu} \tag{2}$$

By fitting the experimental ΔE data points in Figure 3c with eq 2, we obtain (0.081 ± 0.002) m_0 for $(BTa)_2PbI_4$ and (0.080 ± 0.002) m_0 for $(F_2BTa)_2PbI_4$, where m_0 is the electron rest mass (see Figure S2). For both benzotriazole-based compounds, the reduced effective masses are approximately 12% lower as compared to that of $(PEA)_2PbI_4$. This demonstrates that organic cation templating can be effectively used to tune the reduced effective mass of charge carriers. According to DFT calculations presented in[15] the μ in lead−iodide Ruddlesden−Popper 2D perovskite characterized with $\beta \approx 3°$ and $\delta \approx 0°$ should be in the range of 0.065−0.075 m_0. This is slightly lower than our experimental result of 0.08 m_0, however, it certainly follows the trend emerging from the DFT simulations.

Having determined the μ we go back to the fan chart presented in Figure 3b to estimate the band gap energy. According to eq 1 the Landau levels intercross at 0 T, which provides a direct estimate of E_g. The determined E_g value equals ~2.517 ± 0.002 eV for $(BTa)_2PbI_4$ and ~2.518 ± 0.002 eV for $(F_2BTa)_2PbI_4$, see Figure S3b. The extracted value is in good agreement with the E_g determined from photoluminescence excitation (PLE) spectroscopy, as shown in Figure 3d (for details on PLE measurements see section Materials and Methods). In the PLE spectrum, we observe a maximum at around ~2.518 ± 0.002 eV for $(BTa)_2PbI_4$ and ~2.521 ± 0.003 eV for $(F_2BTa)_2PbI_4$ (shaded region in Figure 3d), which corresponds to the E_g. Finally, having the band gap energy, we estimate the exciton binding energy E_b as the difference between the 1s exciton energy and E_g. We obtain $E_b \approx 206 \pm 2$ meV and $\approx 208 \pm 4$ meV for $(BTa)_2PbI_4$ and $(F_2BTa)_2PbI_4$, respectively (see also Table 1).

The decrease of the exciton reduced mass and exciton binding energy is also reflected in the behavior of the excitonic transition in the magnetic field. In Figure 3e we show the second derivative of reflectivity spectrum in the energy range corresponding to the 1s excitonic transition. In the highest magnetic field of 86 T (top curve), we observe a clear splitting due to the Zeeman effect. The total magnetic field-induced shift of the 1s exciton state δE_{1s} is given by the sum of the Zeeman and diamagnetic contributions:

$$\delta E_{1s} = \pm\frac{1}{2}g\mu_B B + c_0 B^2 \tag{3}$$

where g is the Landé g-factor, μ_B is the Bohr magneton, and c_0 is the diamagnetic coefficient. In Figure S6a we present both Zeemann branches of the 1s excitonic transition. By fitting the

https://doi.org/10.1021/acs.jpcc.4c05300
J. Phys. Chem. C 2024, 128, 17984−17989

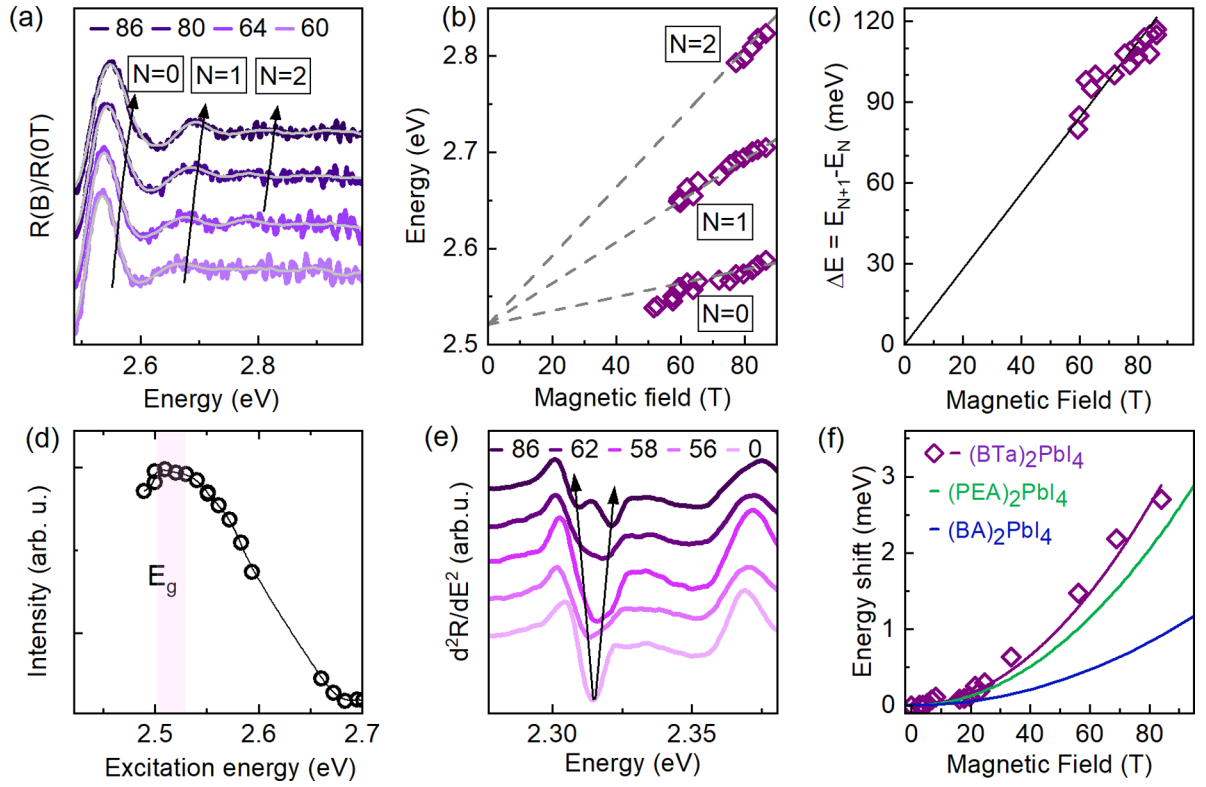

Figure 3. (a) $R(B)/R(0T)$ ratio reflectivity spectrum of $(BTa)_2PbI_4$ at selected magnetic fields. Arrows indicate the evolution of the interband Landau level transitions. (b) Fan chart showing the energy of the interband Landau level transitions as a function of the applied magnetic field B for $(BTa)_2PbI_4$. (c) Energy difference $\Delta E = E_{N+1} - E_N$ between Landau levels as a function of the magnetic field for $(BTa)_2PbI_4$ (purple) along with the fitted line, whose slope is inversely proportional to the effective mass. (d) Photoluminescence excitation (PLE) spectrum of $(BTa)_2PbI_4$. Shaded region indicates the energy position of the band gap E_g. (e) Evolution of the 2nd derivative of the reflectivity spectrum of $(BTa)_2PbI_4$ as a function of the magnetic field. Arrows indicate the 1s exciton resonance split by the Zeeman effect. (f) Energy shift of the 1s exciton as a function of the magnetic field for $(BTa)_2PbI_4$ (points) together with fit (violet line). Green and blue lines are the diamagnetic shifts of $(PEA)_2PbI_4$[15] and $(BA)_2PbI_4$,[17] respectively.

data points with eq 3, we estimate the g-factor ~2.4 ± 0.1 for both samples (see Figure S6b). Furthermore, by averaging the spin-split Zeeman branches, we extract the diamagnetic contribution (the diamagnetic term is the same for both Zeeman-split bands—see eq 3). Data points in Figure 3f show the diamagnetic contribution to the energy shift ΔE_{1s}. This shift is proportional to B^2, and can be modeled with the equation $\Delta E_{1s} = c_0 B^2$. The fitting procedure yields $c_0 = 0.41 \pm 0.03$ $\mu eV/T^2$ for $(BTa)_2PbI_4$ and $c_0 = 0.44 \pm 0.02$ $\mu eV/T^2$ for $(F_2BTa)_2PbI_4$, as shown Figure S2f in SI. All of our findings are summarized in Table 1.

The c_0 coefficient depends on the reduced effective mass μ as $c_0 \sim \frac{1}{\mu^3}$, whereas μ is proportional to the exciton binding energy $E_b \sim \mu$.[39] The determined c_0 values are higher than those reported for $(PEA)_2PbI_4$[15] and $(BA)_2PbI_4$,[17,25] which we plot as green and blue curve in Figure 3f. This corroborates the reduction of the effective mass μ and the related reduction of the exciton binding energy E_b. It is worth noting that c_0 coefficient can serve to quantify the effective mass of the carriers based on the phenomenological scaling law proposed in work[40] :

$$\mu = \alpha\left(\frac{\varepsilon_\infty^2}{c_0}\right) \tag{4}$$

where ε_∞ is the effective dielectric constant (we used the values for 2D perovskites in the range 3.8–4.1), and α is a proportionality factor equal to 0.024. eq 4 yields μ in the range of 0.079–0.086 m_0 in good agreement with our Landau levels analysts providing additional support for our findings.

CONCLUSIONS

In conclusion, our magneto-optical investigation demonstrates the remarkable potential of distortion engineering in 2D perovskite materials, particularly with the introduction of organic cations with strong intermolecular interactions such as benzotriazole-based organic spacers. By investigating $(BTa)_2PbI_4$ and $(F_2BTa)_2PbI_4$, we show that the reduction in octahedral distortion has profound implications for the electronic properties of these materials, leading to a lowering of the reduced effective mass by 12%. This represents the lowest reported effective mass in lead-based 2D perovskites so far. Correspondingly, the band gap energy and the exciton binding energy are also reduced. Importantly, our work highlights the broader applicability of templating techniques to tailor the electronic properties of 2D perovskites. This strategy may be further extended to include tin-based compounds, opening up new avenues for the design and optimization of 2D layered perovskites for various optoelectronic applications.

ASSOCIATED CONTENT

Supporting Information

The Supporting Information is available free of charge at https://pubs.acs.org/doi/10.1021/acs.jpcc.4c05300.

https://doi.org/10.1021/acs.jpcc.4c05300
J. Phys. Chem. C 2024, 128, 17984−17989

Definition of δ angle, crystal structure, reflectivity spectrum, determined the effective mass, diamagnetic coefficient, and band gap of $(F_2BTa)_2PbI_4$; reflectivity spectra of $(BTa)_2PbI_4$ in a magnetic field; detailed uncertainly analysis of Landau level transitions; and determined Zeeman splitting for both samples (PDF)

AUTHOR INFORMATION

Corresponding Author

Mateusz Dyksik − *Department of Experimental Physics, Faculty of Fundamental Problems of Technology, Wrocław University of Science and Technology, 50-370 Wrocław, Poland;* orcid.org/0000-0003-4945-8795; Email: mateusz.dyksik@pwr.edu.pl

Authors

Paulina Peksa − *Department of Experimental Physics, Faculty of Fundamental Problems of Technology, Wrocław University of Science and Technology, 50-370 Wrocław, Poland; Laboratoire National des Champs Magnétiques Intenses, EMFL, CNRS UPR 3228, Université Grenoble Alpes, Université Toulouse, Grenoble and Toulouse 31400, France;* orcid.org/0000-0002-1483-4407

Arthur Maufort − *Hybrid Materials Design, Institute for Materials Research (imo-imomec), Hasselt University, B-3500 Hasselt, Belgium;* orcid.org/0000-0001-9621-6014

Michał Baranowski − *Department of Experimental Physics, Faculty of Fundamental Problems of Technology, Wrocław University of Science and Technology, 50-370 Wrocław, Poland;* orcid.org/0000-0002-5974-0850

Alessandro Surrente − *Department of Experimental Physics, Faculty of Fundamental Problems of Technology, Wrocław University of Science and Technology, 50-370 Wrocław, Poland;* orcid.org/0000-0003-4078-4965

Laurence Lutsen − *Hybrid Materials Design, Institute for Materials Research (imo-imomec), Hasselt University, B-3500 Hasselt, Belgium; Imec-imomec, B-3590 Diepenbeek, Belgium*

Paulina Płochocka − *Department of Experimental Physics, Faculty of Fundamental Problems of Technology, Wrocław University of Science and Technology, 50-370 Wrocław, Poland; Laboratoire National des Champs Magnétiques Intenses, EMFL, CNRS UPR 3228, Université Grenoble Alpes, Université Toulouse, Grenoble and Toulouse 31400, France;* orcid.org/0000-0002-4019-6138

Wouter T. M. Van Gompel − *Hybrid Materials Design, Institute for Materials Research (imo-imomec), Hasselt University, B-3500 Hasselt, Belgium;* orcid.org/0000-0002-8173-5206

Complete contact information is available at: https://pubs.acs.org/10.1021/acs.jpcc.4c05300

Notes

The authors declare no competing financial interest.

ACKNOWLEDGMENTS

P.Pe appreciates the support from the Polish National Agency for Academic Exchange within the Bekker program (grant no.BPN/BEK/2022/1/00120/U/00001). P.Pl acknowledges the National Science Centre, Poland grant no. 2020/38/A/ST3/00214. M.D. acknowledges support from the National Science Centre Poland within the SONATA grant (2021/43/D/ST3/01444). A.S. gratefully acknowledges the support of the National Science Centre, Poland, grant no. 2020/39/D/ST3/03000, A.M. acknowledges the Research Foundation Flanders (FWO) for the funding of his FWO fundamental research PhD grant (1115721N). W.T.M.V.G. and L.L. acknowledge the FWO for the funding of the FWO research projects G043320N and G0A8723N.

REFERENCES

(1) Huo, C.; Cai, B.; Yuan, Z.; Ma, B.; Zeng, H. Two-dimensional metal halide perovskites: theory, synthesis, and optoelectronics. *Small Methods* **2017**, *1*, No. 1600018.

(2) Ghimire, S.; Klinke, C. Two-dimensional halide perovskites: synthesis, optoelectronic properties, stability, and applications. *Nanoscale* **2021**, *13*, 12394−12422.

(3) Smith, I. C.; Hoke, E. T.; Solis-Ibarra, D.; McGehee, M. D.; Karunadasa, H. I. A layered hybrid perovskite solar-cell absorber with enhanced moisture stability. *Angew. Chem., Int. Ed.* **2014**, *53*, 11232−11235.

(4) Marongiu, D.; Saba, M.; Quochi, F.; Mura, A.; Bongiovanni, G. The role of excitons in 3D and 2D lead halide perovskites. *Journal of Materials Chemistry C* **2019**, *7*, 12006−12018.

(5) Chen, Y.; Sun, Y.; Peng, J.; Tang, J.; Zheng, K.; Liang, Z. 2D Ruddlesden−Popper perovskites for optoelectronics. *Adv. Mater.* **2018**, *30*, No. 1703487.

(6) Wu, G.; Liang, R.; Zhang, Z.; Ge, M.; Xing, G.; Sun, G. 2D hybrid halide perovskites: structure, properties, and applications in solar cells. *Small* **2021**, *17*, No. 2103514.

(7) Gao, X.; Zhang, X.; Yin, W.; Wang, H.; Hu, Y.; Zhang, Q.; Shi, Z.; Colvin, V. L.; Yu, W. W.; Zhang, Y. Ruddlesden−popper perovskites: synthesis and optical properties for optoelectronic applications. *Adv. Sci.* **2019**, *6*, No. 1900941.

(8) Hu, J.; Yan, L.; You, W. Two-dimensional organic−inorganic hybrid perovskites: a new platform for optoelectronic applications. *Adv. Mater.* **2018**, *30*, No. 1802041.

(9) Liang, C.; Zhao, D.; Li, Y.; Li, X.; Peng, S.; Shao, G.; Xing, G. Ruddlesden−Popper perovskite for stable solar cells. *Energy & Environmental Materials* **2018**, *1*, 221−231.

(10) Zhang, X.; Ren, X.; Liu, B.; Munir, R.; Zhu, X.; Yang, D.; Li, J.; Liu, Y.; Smilgies, D.-M.; Li, R.; et al. Stable high efficiency two-dimensional perovskite solar cells via cesium doping. *Energy Environ. Sci.* **2017**, *10*, 2095−2102.

(11) Knutson, J. L.; Martin, J. D.; Mitzi, D. B. Tuning the band gap in hybrid tin iodide perovskite semiconductors using structural templating. *Inorganic chemistry* **2005**, *44*, 4699−4705.

(12) Straus, D. B.; Kagan, C. R. Photophysics of Two-Dimensional Semiconducting Organic−Inorganic Metal-Halide Perovskites. *Annu. Rev. Phys. Chem.* **2022**, *73*, 403−428.

(13) Smith, M. D.; Karunadasa, H. I. White-light emission from layered halide perovskites. *Accounts of chemical research* **2018**, *51*, 619−627.

(14) Dyksik, M.; Beret, D.; Baranowski, M.; Duim, H.; Moyano, S.; Posmyk, K.; Mlayah, A.; Adjokatse, S.; Maude, D. K.; Loi, M. A.; et al. Polaron Vibronic Progression Shapes the Optical Response of 2D Perovskites. *Adv. Sci.* **2023**, *11*, No. 2305182.

(15) Dyksik, M.; Duim, H.; Zhu, X.; Yang, Z.; Gen, M.; Kohama, Y.; Adjokatse, S.; Maude, D. K.; Loi, M. A.; Egger, D. A.; et al. Broad tunability of carrier effective masses in two-dimensional halide perovskites. *ACS Energy Letters* **2020**, *5*, 3609−3616.

(16) Dyksik, M.; Wang, S.; Paritmongkol, W.; Maude, D. K.; Tisdale, W. A.; Baranowski, M.; Plochocka, P. Tuning the Excitonic Properties of the 2D (PEA) 2 (MA) n- 1Pb n I3 n+ 1 Perovskite Family via Quantum Confinement. *J. Phys. Chem. Lett.* **2021**, *12*, 1638−1643.

(17) Baranowski, M.; Zelewski, S. J.; Kepenekian, M.; Traoré, B.; Urban, J. M.; Surrente, A.; Galkowski, K.; Maude, D. K.; Kuc, A.; Booker, E. P.; et al. Phase-transition-induced carrier mass enhancement in 2D Ruddlesden−Popper perovskites. *ACS Energy Letters* **2019**, *4*, 2386−2392.

(18) Ng, Y. F.; Febriansyah, B.; Jamaludin, N. F.; Giovanni, D.; Yantara, N.; Chin, X. Y.; Tay, Y. B.; Sum, T. C.; Mhaisalkar, S.; Mathews, N. Design of 2D templating molecules for mixed-dimensional perovskite light-emitting diodes. *Chem. Mater.* **2020**, *32*, 8097−8105.
(19) Wang, J.; Luo, S.; Lin, Y.; Chen, Y.; Deng, Y.; Li, Z.; Meng, K.; Chen, G.; Huang, T.; Xiao, S.; et al. Templated growth of oriented layered hybrid perovskites on 3D-like perovskites. *Nat. Commun.* **2020**, *11*, 582.
(20) Chakraborty, R.; Nag, A. Dielectric confinement for designing compositions and optoelectronic properties of 2D layered hybrid perovskites. *Phys. Chem. Chem. Phys.* **2021**, *23*, 82−93.
(21) Surrente, A.; Baranowski, M.; Plochocka, P. Perspective on the physics of two-dimensional perovskites in high magnetic field. *Appl. Phys. Lett.* **2021**, *118*, 170501.
(22) Pedesseau, L.; Sapori, D.; Traore, B.; Robles, R.; Fang, H.-H.; Loi, M. A.; Tsai, H.; Nie, W.; Blancon, J.-C.; Neukirch, A.; et al. Advances and promises of layered halide hybrid perovskite semiconductors. *ACS Nano* **2016**, *10*, 9776−9786.
(23) Chen, X.; Lu, H.; Wang, K.; Zhai, Y.; Lunin, V.; Sercel, P. C.; Beard, M. C. Tuning spin-polarized lifetime in two-dimensional metal−halide perovskite through exciton binding energy. *J. Am. Chem. Soc.* **2021**, *143*, 19438−19445.
(24) Zhong, X.; Ni, X.; Kaplan, A.; Zhao, X.; Ivancevic, M.; Ball, M. L.; Xu, Z.; Li, H.; Rand, B. P.; Loo, Y.-L. Evolution of the Electronic and Excitonic Properties in 2D Ruddlesden−Popper Perovskites Induced by Bifunctional Ligands. *Adv. Energy Mater.* **2024**, *14*, No. 2304345.
(25) Blancon, J.-C.; Stier, A. V.; Tsai, H.; Nie, W.; Stoumpos, C. C.; Traore, B.; Pedesseau, L.; Kepenekian, M.; Katsutani, F.; Noe, G.; et al. Scaling law for excitons in 2D perovskite quantum wells. *Nat. Commun.* **2018**, *9*, 2254.
(26) Caiazzo, A.; Maufort, A.; van Gorkom, B. T.; Remmerswaal, W. H.; Orri, J. F.; Li, J.; Wang, J.; van Gompel, W. T.; Van Hecke, K.; Kusch, G.; et al. 3D Perovskite Passivation with a Benzotriazole-Based 2D Interlayer for High-Efficiency Solar Cells. *ACS Applied Energy Materials* **2023**, *6*, 3933−3943.
(27) Maufort, A.; Cerdá, J.; Van Hecke, K.; Deduytsche, D.; Verding, A.; Ruttens, B.; Li, W.; Detavernier, C.; Lutsen, L.; Quarti, C. Elucidating the Non-Covalent Interactions that Trigger Interdigitation in Lead-Halide Layered Hybrid Perovskites. *Inorg. Chem.* **2024**, *63*, 5568−5579.
(28) Billing, D. G.; Lemmerer, A. Synthesis, characterization and phase transitions in the inorganic−organic layered perovskite-type hybrids [(CnH2n+ 1NH3) 2PbI4], n= 4, 5 and 6. *Acta Crystallographica Section B: Structural Science* **2007**, *63*, 735−747.
(29) Hansen, K. R.; McClure, C. E.; Colton, J. S.; Whittaker-Brooks, L. Franz-Keldysh and Stark effects in two-dimensional metal halide perovskites. *PRX Energy* **2022**, *1*, No. 013001.
(30) Straus, D. B.; Iotov, N.; Gau, M. R.; Zhao, Q.; Carroll, P. J.; Kagan, C. R. Longer cations increase energetic disorder in excitonic 2D hybrid perovskites. *journal of physical chemistry letters* **2019**, *10*, 1198−1205.
(31) Du, K.-z.; Tu, Q.; Zhang, X.; Han, Q.; Liu, J.; Zauscher, S.; Mitzi, D. B. Two-dimensional lead (II) halide-based hybrid perovskites templated by acene alkylamines: crystal structures, optical properties, and piezoelectricity. *Inorganic chemistry* **2017**, *56*, 9291−9302.
(32) Posmyk, K.; Dyksik, M.; Surrente, A.; Maude, D. K.; Zawadzka, N.; Babiński, A.; Molas, M. R.; Paritmongkol, W.; Maczka, M.; Tisdale, W. A.; et al. Exciton Fine Structure in 2D Perovskites: The Out-of-Plane Excitonic State. *Adv. Opt. Mater.* **2023**, *12*, No. 2300877.
(33) Posmyk, K.; Dyksik, M.; Surrente, A.; Zalewska, K.; Śmiertka, M.; Cybula, E.; Paritmongkol, W.; Tisdale, W. A.; Plochocka, P.; Baranowski, M. Fine Structure Splitting of Phonon-Assisted Excitonic Transition in (PEA) 2PbI4 Two-Dimensional Perovskites. *Nanomaterials* **2023**, *13*, 1119.
(34) Posmyk, K.; Zawadzka, N.; Kipczak, Ł.; Dyksik, M.; Surrente, A.; Maude, D. K.; Kazimierczuk, T.; Babinéski, A.; Molas, M. R.; Bumrungsan, W.; et al. Bright Excitonic Fine Structure in Metal-Halide Perovskites: From Two-Dimensional to Bulk. *J. Am. Chem. Soc.* **2024**, *146*, 4687−4694.
(35) Urban, J. M.; Chehade, G.; Dyksik, M.; Menahem, M.; Surrente, A.; Trippé-Allard, G.; Maude, D. K.; Garrot, D.; Yaffe, O.; Deleporte, E.; et al. Revealing Excitonic Phonon Coupling in (PEA) 2 (MA) n- 1Pb n I3 n+ 1 2D Layered Perovskites. *J. Phys. Chem. Lett.* **2020**, *11*, 5830−5835.
(36) Straus, D. B.; Hurtado Parra, S.; Iotov, N.; Gebhardt, J.; Rappe, A. M.; Subotnik, J. E.; Kikkawa, J. M.; Kagan, C. R. Direct observation of electron−phonon coupling and slow vibrational relaxation in organic−inorganic hybrid perovskites. *J. Am. Chem. Soc.* **2016**, *138*, 13798−13801.
(37) Neutzner, S.; Thouin, F.; Cortecchia, D.; Petrozza, A.; Silva, C.; Kandada, A. R. S. Exciton-polaron spectral structures in two-dimensional hybrid lead-halide perovskites. *Phys. Rev. Mater.* **2018**, *2*, No. 064605.
(38) Sichert, J. A.; Hemmerling, A.; Cardenas-Daw, C.; Urban, A. S.; Feldmann, J. Tuning the optical bandgap in layered hybrid perovskites through variation of alkyl chain length. *APL Mater.* **2019**, *7*, No. 041116.
(39) Miura, N. *Physics of semiconductors in high magnetic fields*; OUP Oxford, 2007; Vol. *15*.
(40) Dyksik, M. Using the Diamagnetic Coefficients to Estimate the Reduced Effective Mass in 2D Layered Perovskites: New Insight from High Magnetic Field Spectroscopy. *International Journal of Molecular Sciences* **2022**, *23*, 12531.

https://doi.org/10.1021/acs.jpcc.4c05300
J. Phys. Chem. C 2024, 128, 17984−17989